Approximate Solution to the Sokolovskiĭ Concave Slope at Limiting Equilibrium

Isaac A. Jeldes, S.M.ASCE[1]; Nicholas E. Vence[2]; and Eric C. Drumm, M.ASCE[3]

Abstract: The growth of precision autoguidance systems on construction equipment suggests that nonplanar slopes and landforms now can be constructed readily. Slopes with concave cross sections not only appear more like natural slopes, but can also have superior stability and erosion resistance. Thus, it is desirable to have the description of concave slopes that provide mechanical stability for a given set of soil properties. In this paper, an approximate solution that defines the geometry of critical concave slopes (factor of safety ≈ 1) in a frictional medium is developed, based on the slip-line field method. The approximate solution is compared with previous numerical results and validated via limit-equilibrium method and FEM analyses. The proposed solution is simple in form, and, when implemented with precision construction equipment, will allow the construction of embankments and reclaimed mine lands that appear more like those in nature and yet are more resistant to erosion. **DOI: 10.1061/(ASCE)GM.1943-5622.0000330.**

Author keywords: Concave slopes; Slope stability; Soil erosion; Slip-line field theory; Critical slope surface.

Introduction

The growth of precision of autoguidance construction equipment and three-dimensional (3D) mapping technology allows more complex nonplanar slopes and landforms to be constructed readily. This can lead to engineered slopes of concave cross sections that appear more like natural slopes and have superior stability and erosion resistance (Schor and Gray 2007). In fact, experimental and numerical simulations have shown that concave slopes lead to less erosion than planar slopes (Meyer and Kramer 1969; Rieke-Zapp and Nearing 2005). The general concept of form follows function is observed in geomorphological evolutionary processes, such as fluvial systems where concave slopes are suggested as the most probable shape in landform evolution (Leopold and Langbein 1962; Miyamoto et al. 2005). Furthermore, slopes subjected to physical weathering seem to evolve into steady-state, concave-like forms to achieve erosional equilibrium (Nash 1980; Pelletier and Rasmussen 2009; Twidale 2007). The use of concave surfaces can become a powerful ecological building technique to reduce sediment yield in constructed embankments, reclaimed mine lands, and highway cut and fill sections, with shapes that appear more like those observed in nature. Thus, it is important to investigate and define the optimum concave shape relative to mechanical slope stability. While computational methods based on limit-equilibrium and limit-analysis techniques (Ahmed et al. 2012; Liu and Zhao 2013; Michalowski 2010) prevail in slope analyses and design, the authors employed a rational mechanics approach based on Sokolovskiĭ's slip-line field theory to define concave slope shapes at critical equilibrium.

Sokolovskiĭ (1960, 1965) found that the slope surface at critical or limiting equilibrium has a concave shape, mathematically described as a function of the Mohr-Coulomb (MC) shear strength parameters and the material unit weight. Because the solution for a nonfrictional soil (i.e., undrained loading conditions) is mathematically straightforward, this study focused on the $c-\phi$ case (ϕ is the soil internal friction angle and c is the soil cohesion), which has no analytical solution. For a soil with $\phi > 0$, $c > 0$, and unit weight $\gamma > 0$, Sokolovskiĭ (1960) implemented a numerical solution reporting the slope surface as a function of the ratio c/γ. This solution, however, has some practical design limitations. The Sokolovskiĭ geometric description of the contour is incomplete, which limits the application to distinct values of ϕ and slope heights $y \cdot c/\gamma$. In this paper, the authors (1) revisit and fully describe Sokolovskiĭ's formulation and solution based on slip-line field theory for a weightless slope ($\gamma = 0$), (2) develop an approximate analytical solution that describes the concave slope at critical equilibrium for a medium with self-weight ($\gamma > 0$), and (3) validate the solution via the limit-equilibrium method (LEM) and the FEM. While the main objective of this work was to provide a rational mathematic description of the critical concave slope shape [factor of safety (FS) = 1], the solution can be extended easily to FS > 1 as needed for design. This issue, along with those related to transient underground water flow and constructability, are addressed briefly.

Background on Slip-Line Field Theory and Characteristic Equations

The slip-line field theory in soil mechanics rests on the assumptions that the soil yield stress is independent of the strain level and that the strain-stress behavior can be described by either elastic perfectly plastic or rigid perfectly plastic idealizations. For frictional materials like soils, the Mohr-Coulomb shear strength expression traditionally has been used as the constitutive law defining the yield or maximum allowable stress. In this context, to bring the body into a limiting equilibrium state or at the verge of flowing plastically, the largest difference between the shear stresses and the shear strength must be zero (Sokolovskiĭ 1960). Expressed in terms of principal stresses

[1]Graduate Research Assistant, Dept. of Civil and Environmental Engineering, Univ. of Tennessee, Knoxville, TN 37996. E-mail: ijeldes@utk.edu

[2]Postdoctoral Research Assistant, Joint Institute of Computational Sciences at Oak Ridge National Laboratory, Oak Ridge, TN 37831-6173. E-mail: nevence@utk.edu

[3]Professor, Dept. of Biosystems Engineering and Soil Science, Univ. of Tennessee, Knoxville, TN 37996 (corresponding author). E-mail: edrumm@utk.edu

Note. This manuscript was submitted on January 8, 2013; approved on June 6, 2013; published online on June 8, 2013. Discussion period open until September 16, 2014; separate discussions must be submitted for individual papers. This paper is part of the ***International Journal of Geomechanics***, © ASCE, ISSN 1532-3641/04014049(8)/$25.00.

$$\max[(\sigma_1 - \sigma_3)\sin(2\lambda - \phi) - \sin\phi(\sigma_1 + \sigma_3 + 2H)] = 0 \quad (1)$$

where σ_1 = major principal stress; σ_3 = minor principal stress (Fig. 1); $H = c \cdot \cot\phi$ = tensile strength of the soil; and λ = angle between the normal to the plane and the major principal direction. Approaching Eq. (1) as a mathematical optimization problem, the limiting condition is reached when

$$2\lambda = \phi + \frac{\pi}{2} \quad (2)$$

which implies that failure or slip line initiates at an angle ε (Fig. 1) inclined at $|45° - \phi/2|$ from the direction of the major principal stress and $|45° + \phi/2|$ from the direction of the minor principal stress. Note that the inclinations of the slip lines are independent of the strain level, which is not always consistent with experimental observations.

Roscoe (1970) concluded that a strain-based approach rather than a stress approach better predicts the inclination of the slip plane, and its magnitude can be approximated by $45° + \psi/2$ (measured from the minor principal direction), where ψ is the dilatancy angle at failure. Later studies on shear band formation in plane-strain experiments confirmed Roscoe's findings (Alshibli and Sture 2000). Nevertheless, this approach is still valid in the context of associated plasticity ($\phi = \psi$), which, for relatively unconfined problems such as slope stability, does not significantly influence the prediction of the FS (Griffiths and Lane 1999) nor the prediction of the critical slip or failure mechanism [except for cases of very low friction angle and high cohesion (Cheng et al. 2007)].

By combining Eqs. (1) and (2), Sokolovskiĭ (1960) obtained the limiting equilibrium in terms of principal stresses as

$$(\sigma_1 - \sigma_3) = \sin\phi(\sigma_1 + \sigma_3 + 2H) \quad (3)$$

If one adopts Sokolovskiĭ (1965) x, y-reference frame (Fig. 1) where the normal of an infinitesimal element located anywhere inside the soil mass is inclined at an angle μ from the x-axis, the slip lines will be inclined at an angle $\xi \pm \varepsilon$ from the x-axis. Then, the equations of limiting stresses can be written in the directions of the adopted reference frame as

$$\sigma_{xx} = \sigma(1 + \sin\phi\cos 2\xi) - H \quad (4)$$

$$\sigma_{yy} = \sigma(1 - \sin\phi\cos 2\xi) - H \quad (5)$$

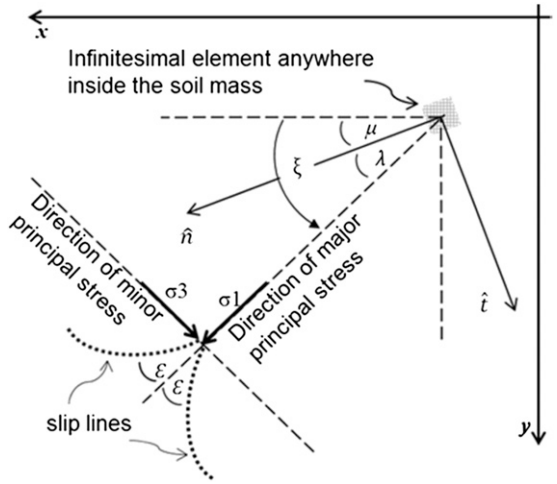

Fig. 1. Orientation of slip lines in a soil mass at limiting equilibrium [adapted from Sokolovskiĭ (1965)]

$$\tau_{xy} = \sigma\sin\phi\sin 2\xi \quad (6)$$

and in the normal $\hat{n}$ and tangential $\hat{t}$ directions (Fig. 1)

$$\sigma_n = \sigma[1 + \sin\phi\cos 2(\xi - \mu)] - H \quad (7)$$

$$\sigma_t = \sigma[1 - \sin\phi\cos 2(\xi - \mu)] - H \quad (8)$$

where σ_{xx} and σ_{yy} = normal limiting stresses acting in the x- and y-directions, respectively; τ_{xy} = shear limiting stress acting on planes perpendicular to the x- and y-axes; σ_n and σ_t = normal limiting stresses acting in the normal $\hat{n}$ and tangential $\hat{t}$ directions, respectively; and $\sigma = 1/2(\sigma_1 + \sigma_3) + H$ = mean stress. When Eqs. (4)–(6) are combined with those of a continuum solid at equilibrium (Malvern 1969), a set of two first-order partial differential equations is obtained, which, upon solution via the method of characteristics (Hill 1950), becomes a set of two differential equations that describe the direction of the slip lines in a soil body, called characteristic equations. Sokolovskiĭ (1965) obtained

$$\frac{dy}{dx} = \tan(\xi \mp \varepsilon) \quad (9)$$

$$d\sigma \mp 2\sigma\tan\phi d\xi = \gamma(dy \mp \tan\phi dx) \quad (10)$$

Elaboration of Sokolovskiĭ Solution for the Critical Slope in a Weightless Medium

By assuming a weightless medium ($\gamma = 0$), the first-order hyperbolic Eq. (10) yields an analytical solution. Here, the authors offer an alternate development of Sokolovskiĭ (1960) analytical solution to this problem, aiming to provide clarity to the mathematical formulation.

Consider the boundary conditions under an external stress q depicted in Fig. 2, where the origin of the rectilinear system of coordinates is set at the intersection of the slope surface and the horizontal ground surface. At the top of the slope (along the horizontal ground surface), the stresses ($\sigma_{xx} = 0, \sigma_{yy} = q, \tau_{xy} = 0$) of the first boundary condition define the y-axis and the x-axis as the major and minor principal directions. Here, $\xi = \pi/2$ and the mean normal stress σ^{surf} from Eq. (5) becomes

$$\sigma^{\text{surf}} = \frac{q + H}{1 + \sin\phi}, \quad \xi = \frac{\pi}{2} \quad (11)$$

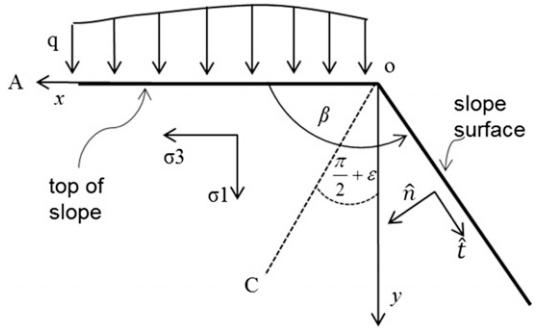

Fig. 2. Critical slope shape (planar) for a weightless medium: inside zone AoC, the principal directions are aligned with the reference frame; on the slope surface, the principal directions are aligned with the normal and tangential directions

Along the slope surface, the stresses redefine the major and minor principal directions as the tangential $\hat{t}$ and normal $\hat{n}$ components, respectively. Therefore, ξ becomes the angle of the slope β measured from the x-axis. By defining the boundary normal stress $\sigma_n = 0$ and $\xi - \mu = \pi/2$, Eq. (7) returns the magnitude of the mean normal stress along the slope surface σ^{cont}

$$\sigma^{\text{cont}} = \frac{H}{1 - \sin\phi}, \quad \xi = \beta \tag{12}$$

Eqs. (11) and (12) establish the boundary conditions of the problem. For a weightless medium ($\gamma = 0$), Eq. (10) becomes

$$\frac{d\sigma}{\sigma} = \pm 2 \tan\phi d\xi \tag{13}$$

Integrating Eq. (13) and imposing the boundary condition along the slope surface from Eq. (12) yields

$$\frac{\cot\phi}{2} \ln\left(\frac{H}{1 - \sin\phi}\right) + c1 = \pm\beta \tag{14}$$

where $c1$ = constant of integration. Eq. (14) reveals the existence of two planes satisfying the stress condition; they have the same absolute inclination and differ only in direction. Choosing $-\beta$ and imposing the surface boundary condition from Eq. (11)

$$c1 = -\frac{\cot\phi}{2} \ln\left(\frac{q + H}{1 + \sin\phi}\right) - \frac{\pi}{2} \tag{15}$$

Substituting Eq. (15) into Eq. (14), β is found to be constant, revealing a planar slope

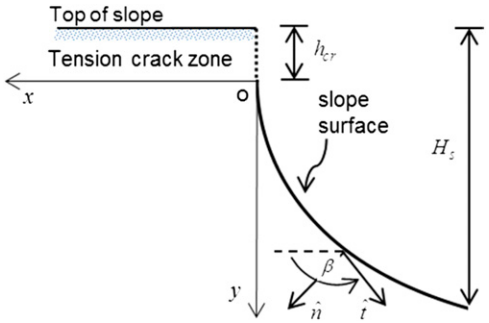

Fig. 3. Slope surface in a medium possessing weight [adapted from Sokolovskiĭ (1965)]

$$\beta = \frac{\pi}{2} + \frac{\cot\phi}{2} \ln\left(\frac{q + H}{H} \frac{1 - \sin\phi}{1 + \sin\phi}\right) \tag{16}$$

which is equivalent to the Sokolovskiĭ (1960) solution, with the discrepancy found only because of the difference in the employed coordinate system. The x-, y-coordinates can be found by solving the first equation of the characteristic system [Eq. (9)], with $\varepsilon = 0$ and $\xi = \beta$ at the slope surface

$$\frac{dy}{dx} = \tan(\beta) \tag{17}$$

The authors emphasize that, for the case of a weightless medium, the slope is constant or planar. However, a medium with self-weight induces changing stress conditions that influence the principal directions, reducing the slope inclination downslope. Sokolovskiĭ's general ($\gamma \neq 0$) solution to Eq. (10) is the result of a numerical boundary-value problem, which has no analytical counterpart. Unfortunately, Sokolovskiĭ's solution is constrained geometrically (i.e., slope height), limited by the ratio c/γ and restricted to specific values of ϕ. Furthermore, extending this solution to other initial conditions requires the reconstruction of the sophisticated boundary-value problem, making its implementation in practical slope design unlikely.

Proposed Solution for the Critical Slope in a Medium with Self-Weight

An analytical approximation for the slope shape of a medium with self-weight is proposed here, based on a weightless medium approximation (WMA). The derivation begins with the initial conditions of the uppermost layer supporting the maximum vertical height of a continuous medium. This vertical height is limited by the height of the tension crack h_{cr} (Terzaghi 1943) and defines the upper portion of the slope (Fig. 3) as a tension zone lying above the x-axis

$$h_{cr} = \frac{2c\cos\phi}{\gamma(1 - \sin\phi)} \tag{18}$$

For the portion of the slope lying below the x-axis, the WMA assumes that the medium can be discretized as a series of finite weightless intervals with constant surface inclination, each supporting a line load representing the self-weight of the layer above.

Fig. 4 depicts a model or analog for a slope composed of multiple layers of weightless media (rigid foam beads), with layers loaded by a line load (frictionless lead sheets). Each new layer adds a finite weight that changes the slope by a finite amount. As the layer thickness $\Delta y \to 0$, the x, y-concave slope emerges. Introducing the

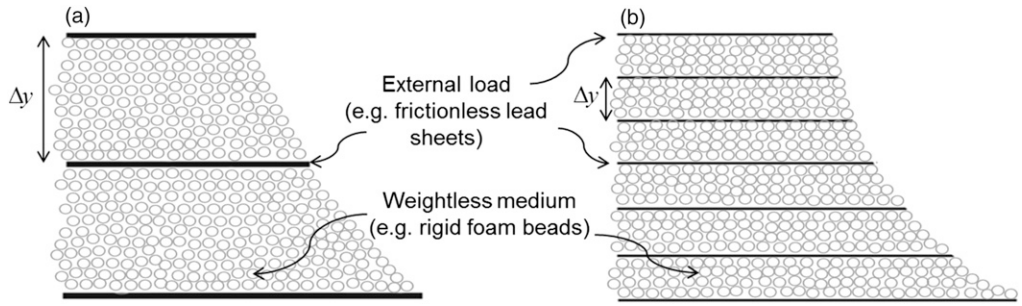

Fig. 4. WMA using discretized weightless medium (e.g., rigid foam beads) supporting thin, external loads (e.g., frictionless lead sheets) separated by a finite interval: (a) coarser discretization; (b) finer discretization

weight of the material as an external stress q, including the weight of the tension zone (γh_{cr}) above the x-axis, and a linearly increasing component (γy) starting from the origin of the reference frame

$$q(y) = (h_{cr} + y)\gamma \tag{19}$$

The authors used the analytical solution from Eq. (16) and replaced the constant load q with Eq. (19). Because $q(y)$ is a function of the vertical direction, y is treated as the independent variable and the angular coordinates transformed to measure the angle from the y-axis. This change of coordinates ($\beta' \to \beta - \pi/2$) makes the slope of the first interval zero rather than infinite

$$\beta'(y) = \frac{\cot\phi}{2}\ln\left(\frac{q(y)+H}{H}\frac{1-\sin\phi}{1+\sin\phi}\right) \tag{20}$$

Accordingly, the first equation of the characteristic [Eq. (9)], after transformation and integration over the closed interval $[0, y]$, becomes

$$x(y) = \int_0^y \tan\left[\beta'(y')\right]dy' \tag{21}$$

The exact solution to Eq. (21) involves a Gauss hypergeometric function ${}_2F_1$ with complex (real and imaginary) arguments. If, as a first approximation, one takes only the real component $[x_{\mathbb{R}}(y)]$ of Eq. (21), it can be seen (Fig. 5) that a concave slope is depicted; however, this solution does not satisfy the critical equilibrium requirement. The discrepancy between Sokolovskiĭ's critical slope and $x_{\mathbb{R}}(y)$ is illustrated in Fig. 5 [with $x_{\mathbb{R}}(y)$ plotted in the negative side of x-axis to match Sokolovskiĭ]. Notice that $x_{\mathbb{R}}(y)$ soon diverges into a horizontal asymptote corresponding to an infinite slope ($\Delta x/\Delta y \to \infty$). The resolution of this infinite-slope problem lies in a second approximation.

Whereas the first WMA is a physical discretization and modification of Eq. (10), the second approximation is a mathematical modification of Eq. (21), via examination of the Taylor series of the tangent of an angle α

$$\tan(\alpha) = \alpha + \frac{\alpha^3}{3} + \frac{2\alpha^5}{15} + O(\alpha^7) \tag{22}$$

with $O(\alpha^7)$ representing truncation of the series from the seventh order. The higher-order terms make the Taylor expansion diverge sooner near $\alpha = \pm\pi/2$. This effect is minimized by removing the high-order terms, replacing $\tan(\alpha) \to \alpha$. Applying the Taylor expansion without the high-order terms reduces Eq. (21) to

$$x(y) = \int_0^y \beta'(y')dy' \tag{23}$$

which has the following analytical solution:

$$x(y) = \begin{cases} 0, & -h_{cr} \le y \le 0 \\ A\left[\sigma_y(B-1)(\cos ec\phi - 1) + H\,B(\cos ec\phi + 1)\right], & y > 0 \end{cases} \tag{24}$$

where

$$A = \frac{\cos\phi}{2\gamma(1-\sin\phi)} \tag{25}$$

$$B = \ln\left[\frac{\sigma_y}{H}\left(\frac{1-\sin\phi}{1+\sin\phi}\right)+1\right] = \ln\left[\frac{\sigma_y}{H}K_a + 1\right] \tag{26}$$

$$\sigma_y = \gamma y \tag{27}$$

$$H = c\cot\phi \tag{28}$$

Notice that the factor B is a function of the Rankine (1857) active coefficient of earth pressure $K_a = (1-\sin\phi)/(1+\sin\phi)$. The proposed solution describes a critical slope surface in the quadrant where x-axis and y-axis are positive, with the tension zone h_{cr} above the x-axis from the origin to the point of coordinates (0, $-h_{cr}$).

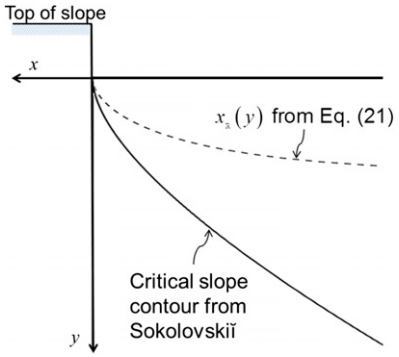

Fig. 5. Sokolovskiĭ's critical slope versus the real (nonimaginary) component of the solution of Eq. (21)

Validation of the WMA Solution

Comparisons between the concave slope surface from the proposed solution [Eq. (24)] and the Sokolovskiĭ (1960) numerical approach were conducted in terms of geometry, critical FS, and failure mechanism. For comparison, the results from Eq. (24) were plotted in the negative side of the x-axis to match Sokolovskiĭ's results. Concave slopes for the range of ϕ and c/γ typically observed in soils were employed here. For fine-grained soils, the range $c = 5-40$ kN/m^2 covered the majority of cases reported by Mesri and Abdelghaffar (1993), and $\gamma = 10-23$ kN/m^3 covered most materials from clays to coarse granular soils (Naval Facilities Engineering Command 1986). Thus, $\phi = 20, 30$, and $40°$, and $c/\gamma = 0.2, 1, 2, 3$, and 4 m were employed to compare Sokolovskiĭ (1960) with the proposed solution. The total vertical slope height (H_s) employed was the maximum reported by Sokolovskiĭ (1960) for the selected range of c/γ (Table 1). The influence of H_s over the computed FS and failure mechanisms is discussed subsequently.

Geometry of the Concave Slopes

The slope surfaces for $\phi = 30°$ and for $c/\gamma = 2$ m are compared in Fig. 6 for a maximum $H_s = 47$ m; slopes for $\phi = 20, 30$, and $40°$ are compared in terms of nondimensional coordinates ($x \cdot \gamma/c$, $y \cdot \gamma/c$) in Fig. 7. For all combinations of ϕ and c/γ, a very close agreement at the upper portion of the slope was observed, whereas differences appeared at the lower portion of the slope. The amount of variation seemed to depend only on the value of ϕ, with best geometric agreement found for $20° \le \phi \le 30°$, which is the range found in many fine-grained soils. Nevertheless, as discussed subsequently,

Table 1. Maximum Values of H_s (m) Reported by Sokolovskiĭ [data from Sokolovskiĭ (1960)] and Used in Stability Analyses

	Internal friction angle ϕ (degrees)		
c/γ (m)	20	30	40
0.2	3.8	5.3	7.1
1.0	19	26	35
2.0	38	53	71
3.0	57	79	106
4.0	76	105	141

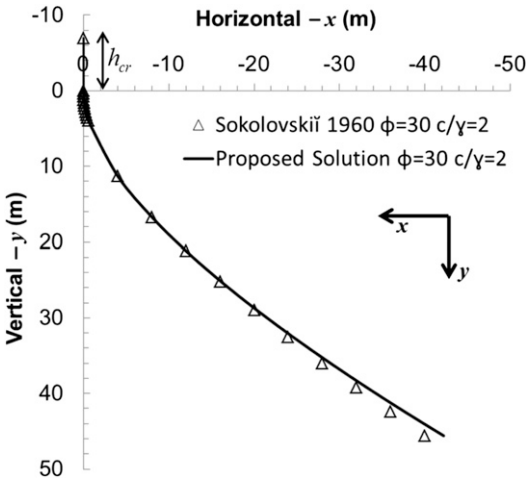

Fig. 6. Comparison of Sokolovskiĭ (1960) numerical solution and the proposed analytical solution for $\phi = 30°$ and $c/\gamma = 2$ m

these geometric variances only induced a minor difference in stability, because, regardless of the value of ϕ, the critical failure mechanism developed in the upper zone of close agreement between the solutions.

Critical FS and Observed Failure Mechanisms

Differences in stability between the two approaches were investigated via FEM and LEM. FEM analyses were computed using the software *Phase2 7.0* and LEM analyses using the software *Slide 6.0*. In the FEM model, a nonassociated flow rule with $\psi = 0$ was employed to avoid effects of computation domain size (Cheng et al. 2007) and to limit the overprediction of dilation (Griffiths and Lane 1999). Also, nominal values for Young's modulus ($E = 2 \times 10^4$ kPa) and Poisson's ratio ($\upsilon = 0.3$) were used, because they play a minor role in the calculation of the FS (Cheng et al. 2007; Griffiths and Lane 1999). In the LEM analyses, the simplified Bishop's method was used with 495,000 critical surfaces analyzed.

A comparison of the computed FS via LEM are reported in Table 2; the FEM results for Sokolovskiĭ's and the proposed solutions when $\phi = 30°$ and $c/\gamma = 2$ m are shown in Figs. 8 and 9, respectively. Very similar results in terms of FS were obtained from FEM and LEM approaches. For all combinations of ϕ and c/γ, the computed critical FS did not differ more than 4% between the proposed and Sokolovskiĭ's solutions. More importantly, all computed FS approximated 1, which is consistent with the limiting strength condition and confirms the appropriateness of Eq. (24). For the investigated range of ϕ, the proposed solution did not deviate more than 6% from the theoretical FS = 1, which can be considered a minor difference in terms of practical applications in geotechnical design.

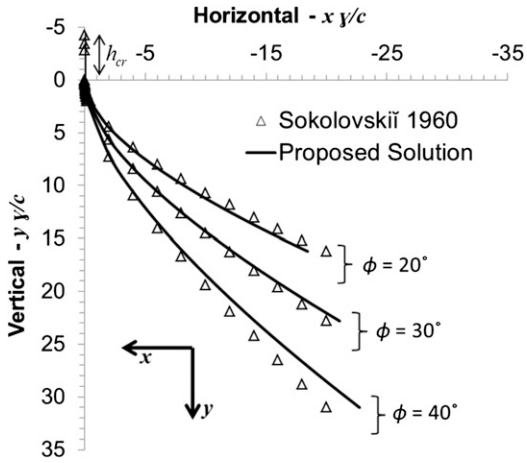

Fig. 7. Comparison of Sokolovskiĭ (1960) numerical solution and the proposed analytical solution in dimensionless coordinates for $\phi = 20$, 30, and 40°

Effects of Slope Height on Failure Mechanisms and FS Obtained from the Proposed Solution

To investigate the effects of the slope height H_s on the stability of the proposed concave slopes, LEM stability analyses were conducted for different values of ϕ, c/γ, and H_s.

Analyses of the results indicated the existence of a limiting slope height (h_L) at which the failure mechanism of the proposed concave slope changed. Concave slopes with heights $H_s < h_L$ developed toe-failure mechanisms, whereas those with $H_s > h_L$ developed face-failure mechanisms (Fig. 10). The change in failure mechanism naturally altered the computed FS, as illustrated in Fig. 11 for the $\phi = 20°$ case. Concave slopes with $H_s < h_L$ tended to have slightly greater FS, which only in a few cases exceeded the theoretical FS = 1 by more than 10%. As H_s approached h_L, the FS decreased until it reached a steady value (FS $\approx$ 1) that remained constant for all $H_s > h_L$. This steady equilibrium condition coincided with a somewhat steady position of the critical failure surface; therefore, h_L defines the height of the failure surface for larger concave slopes. Similar analyses on concave slopes, with $\phi = 30$, 38, and 45°, not only yielded equivalent results but also showed that h_L can be approximated as a linear function of c/γ only (Fig. 12). Over 99% of the variability in h_L can be explained by the linear relationship $h_L = 15.8\ c/\gamma + 0.3$, which can be used to estimate the most likely failure mechanism of a concave slope.

Discussion and Conclusions

Concave slope shapes mimic the landforms observed in nature, and have been determined to be less prone to erosion and sediment production. A mathematical description of the concave slope surface at limiting equilibrium was developed by Sokolovskiĭ (1960), but the characteristic equations must be solved numerically for the most relevant cases, i.e., frictional soils with self-weight ($\phi > 0$, $\gamma > 0$). The lack of an analytical solution limits the application of concave slopes in practice.

In this paper, the authors offer an analytical mathematical approximation for the $\phi > 0$ and $\gamma > 0$ case, to obtain concave slopes at critical equilibrium, for any combination of ϕ, c, and γ. This

Table 2. Comparison of Stability between Proposed Approximate Solution and Sokolovskiĭ (1960) Solution from LEM

	Internal friction angle ϕ (degrees)					
	20		30		40	
c/γ (m)	Proposed approximate	Sokolovskiĭ (1960)	Proposed approximate	Sokolovskiĭ (1960)	Proposed approximate	Sokolovskiĭ (1960)
0.2	1.00	1.04	1.04	1.03	1.06	1.03
1.0	1.00	1.04	1.04	1.03	1.06	1.03
2.0	1.00	1.04	1.04	1.03	1.06	1.03
3.0	1.00	1.04	1.04	1.03	1.06	1.03
4.0	1.00	1.04	1.04	1.03	1.06	1.03

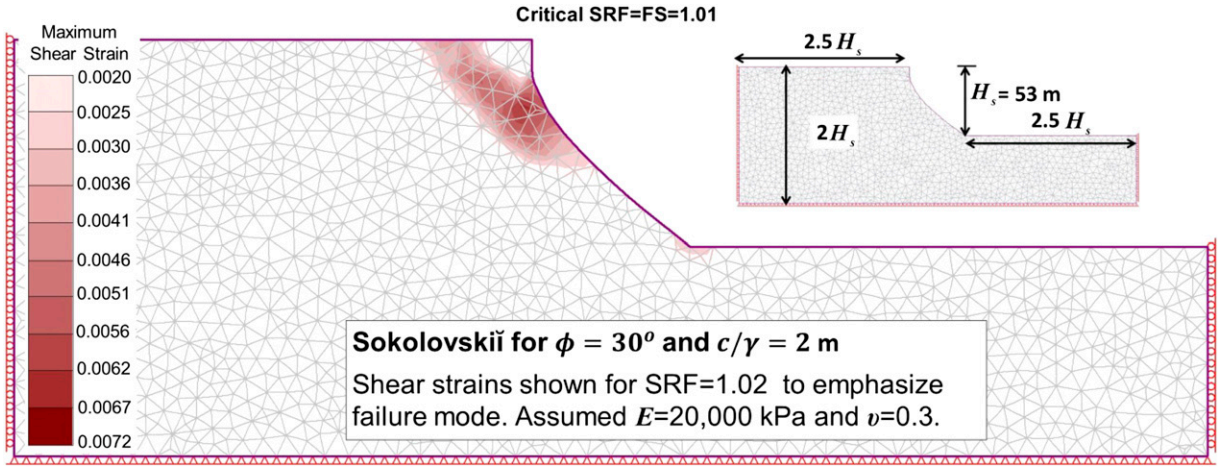

Fig. 8. FEM results in terms of shear strains for the Sokolovskiĭ (1960) critical concave slope

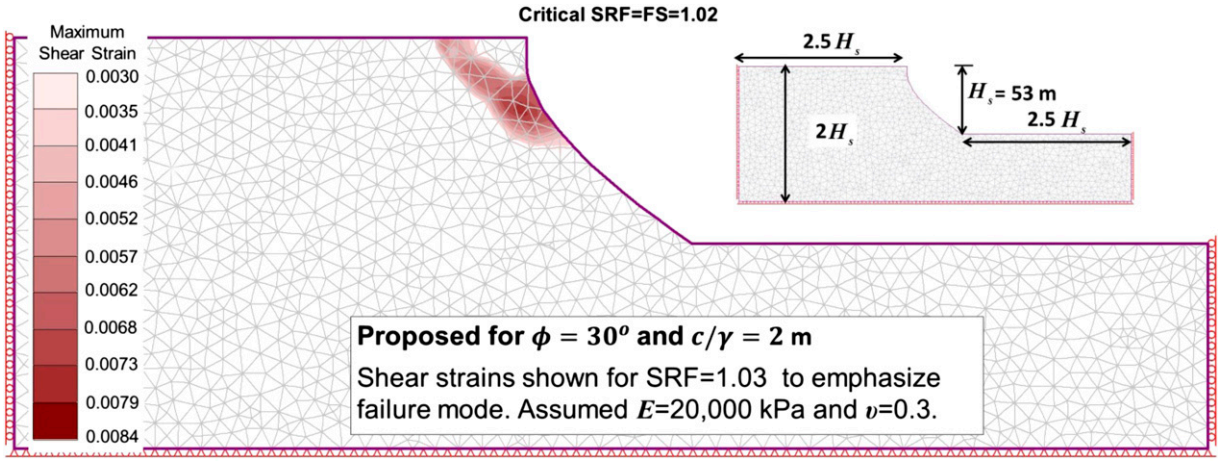

Fig. 9. FEM results in terms of shear strains for the proposed critical concave slope

solution was based on the Sokolovskiĭ solution for a weightless ($\gamma = 0$) medium. The approximation transformed a set of differential equations into a single algebraic expression, which can be used more readily in slope design with no need to reconstruct Sokolovskiĭ's sophisticated numerical boundary-value problem for the $\gamma > 0$ case. The given solution is simple, effective, and it was shown to provide good agreement with Sokolovskiĭ's numeric approach. Unlike Sokolovskiĭ's tabulated values, the proposed solution can be used for any desirable maximum value of H_s or any value of ϕ. In theory, every point of the slope surface depicted by Eq. (24) should be in limiting equilibrium such that, independent of the size of the physical domain, the FS approximates 1. Nevertheless, small deviations arise owing to the approximate nature of the solution. Though associated with the mode of failure, these deviations are small for geotechnical applications and indicate that the stability of the proposed critical concave slopes will range from FS = 1−1.1 for the majority of cases.

Although the solution for the concave slope was developed in terms of the critical slope shape (FS = 1), the proposed solution may be used as a baseline for practical applications. For design, a given FS can be obtained if a strength-reduction factor (Griffiths and Lane 1999; Spencer 1967) equal to the desired FS is used with the

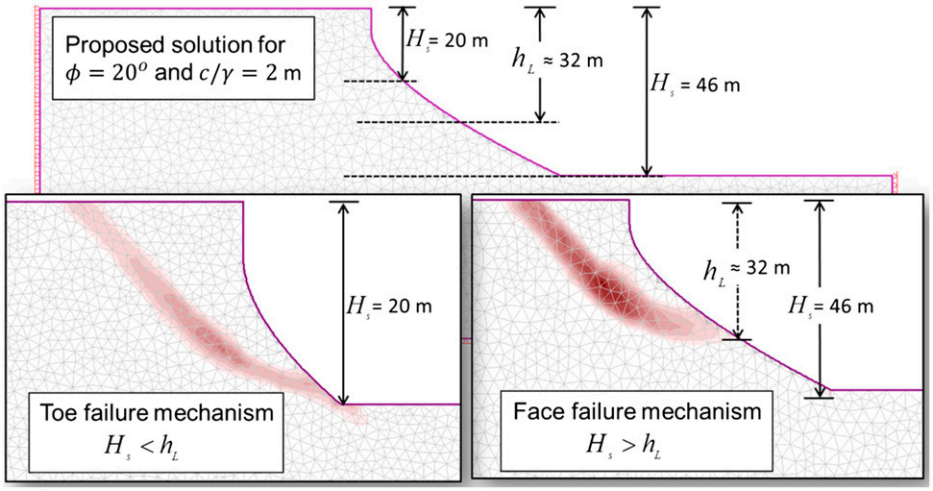

Fig. 10. Modes of failure depicted in the form of shear bands (maximum shear strains) as observed in concave slopes (FEM); for $\phi = 20°$ and $c/\gamma = 2$ m, and two values of H_s

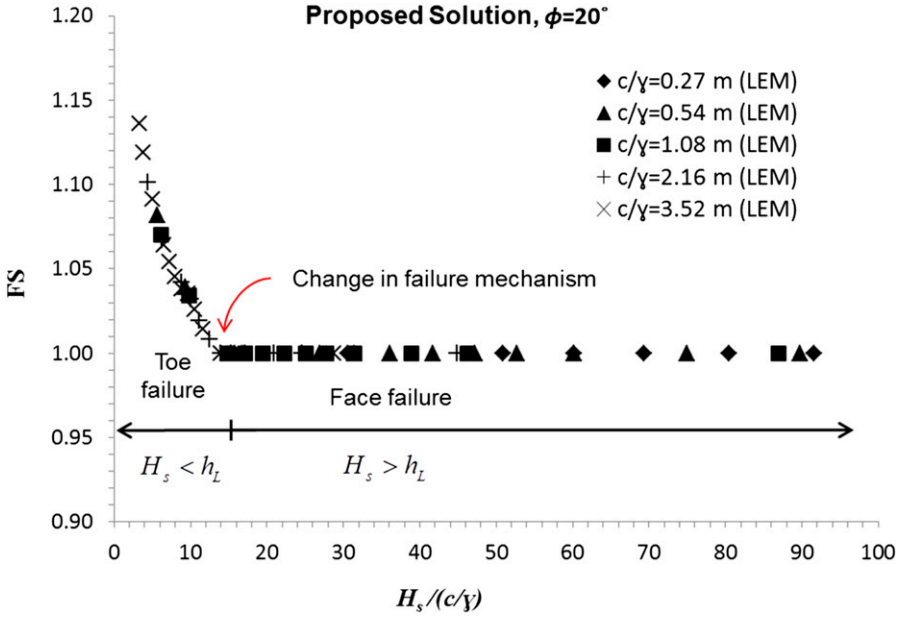

Fig. 11. Computed FS (LEM) on concave slopes with different vertical heights H_s and c/γ for $\phi = 20°$

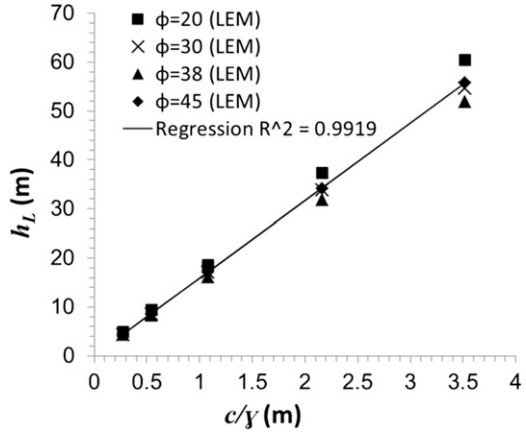

Fig. 12. Relationship between the limiting height h_L and c/γ

proposed solution. The effects of an external semiinfinite surcharge (q_e) acting on the ground surface can be included by adding q_e to the right side of Eq. (19) and modifying Eq. (18) as $h_{cr} = 2c \cos\phi/[\gamma(1 - \sin\phi)] - q_e/\gamma$. Once the desired concave shape is defined, the effects of transient groundwater flow can be investigated using commercial slope stability software. Whereas the successful construction of concave slopes depends on the precision of the employed construction equipment, the increasing precision and availability of GPS-based autoguidance equipment (Koehrsen et al. 2001) makes the construction of concave slopes possible. Nevertheless, in actual slope construction, the sharp bluff at the top (the tension crack zone) is not likely to be constructed because it may erode over time; instead this would be rounded for a more natural appearance, which would decrease the destabilizing forces and add conservatism to concave slope performance.

References

Ahmed, A., Ugai, K., and Yang, Q. Q. (2012). "Assessment of 3D slope stability analysis methods based on 3D simplified Janbu and Hovland methods." *Int. J. Geomech.*, 10.1061/(ASCE)GM.1943-5622.0000117, 81–89.

Alshibli, K. A., and Sture, S. (2000). "Shear band formation in plane strain experiments of sand." *J. Geotech. Geoenviron. Eng.*, 10.1061/(ASCE)1090-0241(2000)126:6(495), 495–503.

Cheng, Y. M., Lansivaara, T., and Wei, W. B. (2007). "Two-dimensional slope stability analysis by limit equilibrium and strength reduction methods." *Comput. Geotech.*, 34(3), 137–150.

Griffiths, D. V., and Lane, P. A. (1999). "Slope stability analysis by finite elements." *Geotechnique*, 49(3), 387–403.

Hill, R. (1950). *The mathematical theory of plasticity*, Clarendon Press, Oxford, U.K.

Koehrsen, C. L., Sahm, W. C., and Keefer, C. W. (2001). "GPS-based earthmoving for construction." *Lect. Notes Comput. Sci.*, 2181, 4–17.

Leopold, L. B., and Langbein, W. B. (1962). *The concept of entropy in landscape evolution*, U.S. Dept. of the Interior, Washington, DC.

Liu, F., and Zhao, J. (2013). "Limit analysis of slope stability by rigid finite-element method and linear programming considering rotational failure." *Int. J. Geomech.*, 10.1061/(ASCE)GM.1943-5622.0000283, 827–839.

Malvern, L. E. (1969). *Introduction to the mechanics of a continuous medium*, Prentice Hall, Englewood Cliffs, NJ.

Mesri, G., and Abdel-Ghaffar, M. E. M. (1993). "Cohesion intercept in effective stress-stability analysis." *J. Geotech. Engrg.*, 10.1061/(ASCE)0733-9410(1993)119:8(1229), 1229–1249.

Meyer, L. D., and Kramer, L. A. (1969). "Erosion equations predict land slope development." *Agric. Eng.*, 50(9), 522–523.

Michalowski, R. L. (2010). "Limit analysis and stability charts for 3D slope failures." *J. Geotech. Geoenviron. Eng.*, 10.1061/(ASCE)GT.1943-5606.0000251, 583–593.

Miyamoto, H., Baker, V., and Lorenz, R. (2005). "Entropy and the shaping of the landscape by water." Chapter 11, *Non-equilibrium thermodynamics and the production of entropy: Life, earth, and beyond*, A. Kleidon and R. Lorenz, eds., Springer, Berlin, 135–146.

Nash, D. (1980). "Forms of bluffs degraded for different lengths of time in Emmet County, Michigan, USA." *Earth Surf. Processes Landforms*, 5(4), 331–345.

Naval Facilities Engineering Command. (1986). *Soil mechanics: NAVFAC DM 7.01—Soil mechanics*, U.S. Government Printing Office, Alexandria, VA.

Pelletier, J. D., and Rasmussen, C. (2009). "Quantifying the climatic and tectonic controls on hillslope steepness and erosion rate." *Lithosphere*, 1(2), 73–80.

Phase2 7.0 [Computer software]. Toronto, Rocscience.

Rankine, W. J. M. (1857). "On the stability of loose earth." *Phil. Trans. R. Soc. Lond.*, 147, 9–27.

Rieke-Zapp, D. H., and Nearing, M. A. (2005). "Slope shape effects on erosion." *Soil Sci. Soc. Am. J.*, 69(5), 1463–1471.

Roscoe, K. H. (1970). "The influence of strains in soil mechanics." *Geotechnique*, 20(2), 129–170.

Schor, H. J., and Gray, D. H. (2007). *Landforming: An environmental approach to hillside development, mine reclamation and watershed restoration*, Wiley, Hoboken, NJ.

Slide 6.0 [Computer software]. Toronto, Rocscience.

Sokolovskiĭ, V. V. (1960). *Statics of soil media*, Butterworths Scientific Publications, London.

Sokolovskiĭ, V. V. (1965). *Statics of granular media*, Pergamon Press, Oxford, U.K.

Spencer, E. (1967). "A method of analysis of the stability of embankments assuming parallel inter-slice forces." *Geotechnique*, 17(1), 11–26.

Terzaghi, K. (1943). *Theoretical soil mechanics*, Wiley, New York.

Twidale, C. R. (2007). "Backwearing of slopes—The development of an idea." *Cuaternario y Geomorfologia*, 21(1–2), 135–146.